

NMR investigations unveil phase composition–property correlations in $\text{Sr}_{0.55}\text{Na}_{0.45}\text{SiO}_{2.775}$ fast ion conductor

P. Lokeswara Rao ^{a,b}, Bholanath Pahari ^{c,*}, M. Shivanand ^d, Tukaram Shet ^d, K.V. Ramanathan ^{a,*}

^a NMR Research Centre, Indian Institute of Science, Bangalore, 560012, India

^b Physics Department, Indian Institute of Science, Bangalore, 560012, India

^c Department of Physics, Goa University, Taleigao Plateau, Goa, 403206, India

^d Materials Research Centre, Indian Institute of Science, Bangalore, 560012, India

ARTICLE INFO

Article history:

Received 30 January 2017

Received in revised form

3 May 2017

Accepted 10 May 2017

Available online 12 May 2017

Keywords:

Solid-state NMR

3QMAS NMR

Fast ion conductor

ABSTRACT

This paper reports results of ^{23}Na and ^{29}Si solid-state NMR investigations carried out on sodium strontium silicate ion conductor, $\text{Sr}_{0.55}\text{Na}_{0.45}\text{SiO}_{2.775}$ and presents the first experimental evidence to show that different synthesis conditions induce multiple devitrified phases. Along with 1-dimensional NMR, ^{23}Na MQMAS spectra have been used to identify the phases corresponding to polymorphs of $\text{Na}_2\text{Si}_2\text{O}_5$, in addition to the crystalline SrSiO_3 and the glass/amorphous $\text{Na}_2\text{Si}_2\text{O}_5$ phases. The surprising observation of about an order of magnitude higher ionic conductivity achieved in devitrified samples is attributed to the growth of the crystalline δ - $\text{Na}_2\text{Si}_2\text{O}_5$ phase within the amorphous $\text{Na}_2\text{Si}_2\text{O}_5$ phase domains, identified using NMR. Together with XRD and conductivity measurement data, the study leads to the identification of the chemical phase composition and an understanding of the composition–property–structure correlation in this material. Present findings, while do not show any evidence of Na doping in the SrSiO_3 phase confirming earlier reports, explain the large discrepancy in the conductivity reported in the literature.

© 2017 Elsevier Inc. All rights reserved.

1. Introduction

Solid oxide fast ion conductors play an important role as electrolyte material for solid oxide fuel cells (SOFC) [1–3]. Recent reports of high ionic conductivity found in the new family of materials bearing the general formula $\text{Sr}_{1-x}\text{Na}_x\text{SiO}_{3-0.5x}$ (SNS) has generated much excitement in the scientist community and it has been demonstrated that the SNS material would be a potential solid electrolyte for intermediate temperature-solid oxide fuel cells (IT-SOFCs) [4–6]. Numerous investigations have been carried out on this family of materials [7–17] and it has been concluded that SNS materials, in general, comprise of two phases: an insulating crystalline SrSiO_3 phase and a Na-ion conducting glass/amorphous $\text{Na}_2\text{O} \cdot 2\text{SiO}_2$ (AM- $\text{Na}_2\text{Si}_2\text{O}_5$) phase. Thus, the high conductivity observed in SNS materials essentially stems from the AM- $\text{Na}_2\text{Si}_2\text{O}_5$ phase. However, there is a large discrepancy in the conductivity reported in the literature for the SNS materials. An ionic conductivity of $10^{-2} \text{ S.cm}^{-1}$ at 525 °C was reported for the first time by Singh et al. [4] on the highest Na-doped composition

of $\text{Sr}_{0.55}\text{Na}_{0.45}\text{SiO}_{2.775}$. Whereas other groups measured almost one order less ionic conductivity on the compound with same nominal composition [9,10]. This discrepancy may arise due to different thermal history leading to devitrification of the amorphous fraction of the samples and hence further investigations are needed.

NMR is an ideal technique to probe the local structure in amorphous and/or crystalline phases of materials [18–20]. To obtain insights into the structure–property correlation in the SNS materials we utilize here ^{23}Na and ^{29}Si NMR spectroscopy extensively. Along with 1-dimensional magic angle spinning (MAS) NMR spectra, we have also carried out ^{23}Na MQMAS studies of these materials. We focus on the highest Na-doped composition of $\text{Sr}_{0.55}\text{Na}_{0.45}\text{SiO}_{2.775}$ (SNS45), prepared through two different synthesis routes. Choice of the highest Na-doped composition also ensures best possible signal-to-noise ratios for ^{23}Na 1D MAS and MQMAS NMR measurements. ^{23}Na , ^{29}Si MAS NMR results obtained in a devitrified form of SNS45 and pure glass/amorphous $\text{Na}_2\text{O} \cdot 2\text{SiO}_2$ are also presented to support the discussion and to show the evolutions of crystalline and amorphous phases. Finally, the NMR experimental results are corroborated with the ionic conductivity data.

* Corresponding authors.

E-mail addresses: bholanath.pahari@unigoa.ac.in (B. Pahari), kvr@nrc.iisc.ernet.in (K.V. Ramanathan).

2. Experimental

Samples with nominal composition $\text{Sr}_{1-x}\text{Na}_x\text{SiO}_{3-0.5x}$ ($x = 0.45$) were synthesized by solid state reaction method using SrCO_3 , Na_2CO_3 and SiO_2 powders. In the first try, the well-mixed powder was pelletized followed by calcination at 1050°C for 10 h. Then half-calcined pellets were crushed into fine powder, re-pelletized and kept at 1050°C for another 10 h. Sample prepared by this two-step heating procedure will be called as SNS45-A. In the second try, the well-mixed powders of starting materials were pelletized and heated at 1050°C for 20 h. Sample prepared by this single step heating method will be called as SNS45-B. Pure glass/amorphous $\text{Na}_2\text{O} \cdot 2\text{SiO}_2$, which will be denoted as AM- $\text{Na}_2\text{Si}_2\text{O}_5$, was prepared by the melt quench method. A devitrified form, SNS45-B $650^\circ\text{C}/12\text{ h}$ was obtained after heating the sample of SNS45-B at 650°C for 12 h. Further details of sample preparation processes are presented in the [Supplementary Content \(SC\)](#). The phase compositions of each of the samples were examined with powder X-ray diffraction (XRD) and the XRD patterns of the samples investigated in this work are shown in SC as [Figs. S1 and S2](#). Conductivity measurements were carried at various temperatures (30°C – 500°C) using an impedance analyser operating in the frequency range of 40 Hz to 10 MHz (further details are given in SC).

All ^{23}Na and ^{29}Si magic-angle spinning (MAS) solid state NMR experiments were carried out at 11.7 T using Bruker Avance III 500 MHz spectrometer. ^{29}Si NMR spectra were recorded using sample filled in 7 mm zirconia rotors spinning at 6 kHz MAS. A 5 μs r.f. pulse was used to record the ^{29}Si NMR spectra employing an r.f. field amplitude of 42 kHz. A relaxation delay of 300 s was chosen for the experiments, which revealed the presence of the sharp component of the NMR spectrum. The broad component was visible for much shorter delays. The result of the spin-lattice relaxation time measurement shown in the supplementary content as [Fig. S3](#) gave an estimate of the T_1 values of the broad and the sharp component of the signal as 2.5 s and 2000 s respectively. The ^{29}Si chemical shifts are quoted relative to tetramethylsilane. ^{23}Na MAS NMR experiments were performed using a 3.2 mm rotor filled with the sample and spinning at 22 kHz. ^{23}Na spectra were obtained using a short r.f. pulse of width 0.45 μs employing an r.f. field amplitude of 92 kHz and a relaxation delay of 1 s. A Z-filter triple-quantum MAS (3QMAS) NMR pulse sequence was employed

to obtain ^{23}Na two-dimensional 3QMAS NMR spectra. R.f. pulses of width 3.8 μs and 1.8 μs with an r.f. field amplitude of 92 kHz were used respectively to excite and to reconvert 3Q coherences. After a z-filter delay of 45 μs a central-transition (CT) selective pulse of width 9 μs at an r.f. amplitude of 14 kHz was employed. All the ^{23}Na spectra were calibrated with respect to 1 M NaCl solution. Deconvolutions of 1D ^{29}Si , ^{23}Na MAS NMR spectra were made with the Dmfit program [21].

3. Results and discussion

3.1. Phase identification with ^{29}Si MAS NMR

^{29}Si MAS NMR spectra of SNS45-A and SNS45-B are plotted together with that of AM- $\text{Na}_2\text{Si}_2\text{O}_5$ and SNS45-B $650^\circ\text{C}/12\text{ h}$ in [Fig. 1](#). The figure also shows the result of the deconvolution of the spectra carried out using the Gaussian line shape functions to model Q^n units of amorphous phase and mixed Gaussian/Lorenzian line shape functions to model crystalline peaks. The peak positions and the full width at half maxima (FWHM) for each of the samples are listed in [Table 1](#). In the case of both SNS45-A [[Fig. 1\(a\)](#)] and SNS45-B [[Fig. 1\(b\)](#)] four peaks are identified. These are centred at around -77.0 , -85.0 , -88.0 , and -100.0 ppm indicating the presence of four distinct local environments for silicon in these two samples. The spectrum of pure AM- $\text{Na}_2\text{Si}_2\text{O}_5$ [[Fig. 1\(c\)](#)] is composed of three broad Gaussian peaks centred at ≈ -77.0 , -88.0 , and -100.0 ppm correspond to Q^2 -, Q^3 - and Q^4 -units, respectively with the dominant silicate species present in pure AM- $\text{Na}_2\text{Si}_2\text{O}_5$ being the Q^3 -unit, in accordance with results reported earlier [22] for this material. By comparison with these results, we assigned the deconvoluted spectra of SNS45-A, B samples. Based on the peak positions and their full width at half maxima (FWHM), we identify the resonance appearing at around -88.0 ppm in SNS45-A, B samples as the Q^3 -units of AM- $\text{Na}_2\text{Si}_2\text{O}_5$ phase. Similarly, the two other broad peaks appearing at -77.0 ppm and -100.0 ppm are assigned to Q^2 -units and Q^4 -units of AM- $\text{Na}_2\text{Si}_2\text{O}_5$ phase, respectively. The remaining sharp peak appearing at the resonance position of -85.0 ppm corresponds to the crystalline α - SrSiO_3 phase. Present peak assignments are in agreement with the previous reports [9,10,14,17]. Although both the ^{29}Si spectra of SNS45-A and SNS45-B contain similar phases (namely Q^2 -, Q^3 -, Q^4 -units of AM- $\text{Na}_2\text{Si}_2\text{O}_5$ and crystalline α - SrSiO_3 phase), their relative contents

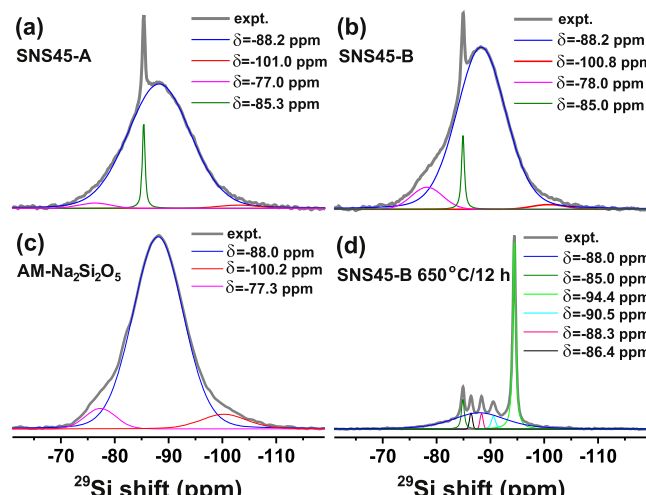


Fig. 1. ^{29}Si NMR spectra of SNS45-A (a), SNS45-B (b), AM- $\text{Na}_2\text{Si}_2\text{O}_5$ (c) and SNS45-B $650^\circ\text{C}/12\text{ h}$ (d) recorded at 11.7 T and 6 kHz MAS frequency. Relevant resonance assignments, obtained from line shape deconvolutions, are displayed with colour lines and their corresponding peak positions are specified. Magenta, Blue and Red traces represent Q^2 -, Q^3 -, Q^4 -units of AM- $\text{Na}_2\text{Si}_2\text{O}_5$ phase. Olive and Green traces represent resonance contributions due to the crystalline α - SrSiO_3 and α - $\text{Na}_2\text{Si}_2\text{O}_5$, Pink and Black traces represent resonance contributions due to two non-equivalent Si environments in crystalline β - $\text{Na}_2\text{Si}_2\text{O}_5$, and Cyan trace represents δ - $\text{Na}_2\text{Si}_2\text{O}_5$ phases, respectively. (For interpretation of the references to colour in this figure legend, the reader is referred to the web version of this article.)

Table 1

Results of ^{29}Si MAS NMR in the samples studied in this paper.

Compound	Phases	One-pulse (1D)	
		δ_{iso} \pm 0.3 ppm	FWHM \pm 0.4 ppm
SNS45-A	Q^2 -unit of AM- $\text{Na}_2\text{Si}_2\text{O}_5$	–77.0	7.0
	Q^3 -unit of AM- $\text{Na}_2\text{Si}_2\text{O}_5$	–88.2	13.7
	Q^4 -unit of AM- $\text{Na}_2\text{Si}_2\text{O}_5$	–101.0	8.9
	SrSiO_3	–85.3	0.6
SNS45-B	Q^2 -unit of AM- $\text{Na}_2\text{Si}_2\text{O}_5$	–78.0	6.8
	Q^3 -unit of AM- $\text{Na}_2\text{Si}_2\text{O}_5$	–88.2	10.7
	Q^4 -unit of AM- $\text{Na}_2\text{Si}_2\text{O}_5$	–100.8	7.5
	SrSiO_3	–85.0	0.65
AM- $\text{Na}_2\text{Si}_2\text{O}_5$	Q^2 -unit of AM- $\text{Na}_2\text{Si}_2\text{O}_5$	–77.3	6.7
	Q^3 -unit of AM- $\text{Na}_2\text{Si}_2\text{O}_5$	–88.0	11.0
	Q^4 -unit of AM- $\text{Na}_2\text{Si}_2\text{O}_5$	–100.2	10.0
	SrSiO_3	–85.0	0.6
SNS45-B 650 °C/12 h	Q^3 -unit of AM- $\text{Na}_2\text{Si}_2\text{O}_5$	–88.0	11.7
	$\alpha\text{-Na}_2\text{Si}_2\text{O}_5$	–94.4	0.7
	$\beta\text{-Na}_2\text{Si}_2\text{O}_5$	–88.3	0.7
	$\delta\text{-Na}_2\text{Si}_2\text{O}_5$	–86.4	0.7
	$\delta\text{-Na}_2\text{Si}_2\text{O}_5$	–90.5	0.9

are slightly different as seen in Fig. 1. Furthermore, the FWHM of the ^{29}Si NMR peak conveys qualitative insights into the glass network (dis)order as it is dictated by the width of distribution of the Si–O–Si/Na bond angles and Si–O distances. Thus, the FWHM of the peak corresponding to the Q^3 -units of AM- $\text{Na}_2\text{Si}_2\text{O}_5$ phase is noticeably higher in SNS45-A compared to that of SNS45-B and pure AM- $\text{Na}_2\text{Si}_2\text{O}_5$ (vide Table 1), thereby indicating higher degree of glass network disordering in SNS45-A sample.

The ^{29}Si MAS NMR spectrum of the devitrified sample of SNS45-B 650 °C/12 h clearly reveals the presence of six resonance contributions as shown by the deconvoluted spectrum in Fig. 1(d). The broad and the sharp resonances at –88.0 ppm and –85.0 ppm, corresponding respectively to the Q^3 -units of AM- $\text{Na}_2\text{Si}_2\text{O}_5$ and the crystalline $\alpha\text{-SrSiO}_3$ phases, which are observed for samples SNS45-A and SNS45-B are present in this case also. However, the relative intensity of AM- $\text{Na}_2\text{Si}_2\text{O}_5$ phase is drastically reduced because of crystallization. Four new sharp resonance contributions are observed additionally. Several crystallographically non-equivalent structures of sodium disilicate are known to exist. Successive heat treatments of the sodium disilicate

glasses show α -, β -, γ -, and $\delta\text{-Na}_2\text{Si}_2\text{O}_5$ as the devitrification products, depending upon the nature of heat treatment. Based on the previously reported [23,24] chemical shift positions, we assign the resonance lines as follows. The peak centred at –94.4 ppm is assigned to crystalline $\alpha\text{-Na}_2\text{Si}_2\text{O}_5$ phase. The lines appearing at –86.4 and –88.3 ppm are assigned to the two non-equivalent Si environments of crystalline $\beta\text{-Na}_2\text{Si}_2\text{O}_5$ phase. The peak at –90.5 ppm is assigned as crystalline $\delta\text{-Na}_2\text{Si}_2\text{O}_5$ phase.

^{29}Si MAS NMR is a good probe to understand the SiO_x moieties present in the SNS45 samples. To gain further insights into the local structure of the SNS materials, we have probed the environment of the sodium atom by utilizing ^{23}Na MAS NMR experiments. Although sodium is relatively easy to study by NMR (the ^{23}Na nucleus has 100% natural abundance and a high magnetogyric ratio), the analysis of the ^{23}Na MAS NMR data in these particular set of samples are challenging because the samples are complex mixtures of crystalline and amorphous phases.

3.2. Phase identification with ^{23}Na MAS NMR

Fig. 2 displays the central transition (CT) region of the ^{23}Na MAS NMR spectra of SNS45-A, SNS45-B, AM- $\text{Na}_2\text{Si}_2\text{O}_5$, and SNS45-B 650 °C/12 h. The spectra of SNS45-A and SNS45-B plotted in Fig. 2(a) and (b), respectively, look significantly different. The ^{23}Na spectra of SNS45-B displays a broad line shape with a long tail at the low frequency side and the line shape is very much similar to that of pure AM- $\text{Na}_2\text{Si}_2\text{O}_5$ in Fig. 2(c). The long tail at the low frequency end results from a distribution of quadrupolar couplings and it indicates the presence of significant structural disorder, and a range of Na sites. The ^{23}Na spectrum of SNS45-A shows a sharp central peak with three recognizable humps on both sides of the peak. However, the basal region of the spectrum is broadened to almost similar extent as of SNS45-B and AM- $\text{Na}_2\text{Si}_2\text{O}_5$. This indicates the presence of more than one phase in SNS45-A sample, possibly a combination of amorphous and early crystalline phases as observed in glass-ceramic materials. The pure AM- $\text{Na}_2\text{Si}_2\text{O}_5$ displays glass transition temperature only at $T_g = 465$ °C and therefore there is always a possibility of partial crystallization at high temperatures while synthesis. Possibility of glass-to-ceramic transition in SNS materials was also indicated previously by others [11,12].

To identify the phases, present in the ^{23}Na spectrum, we have

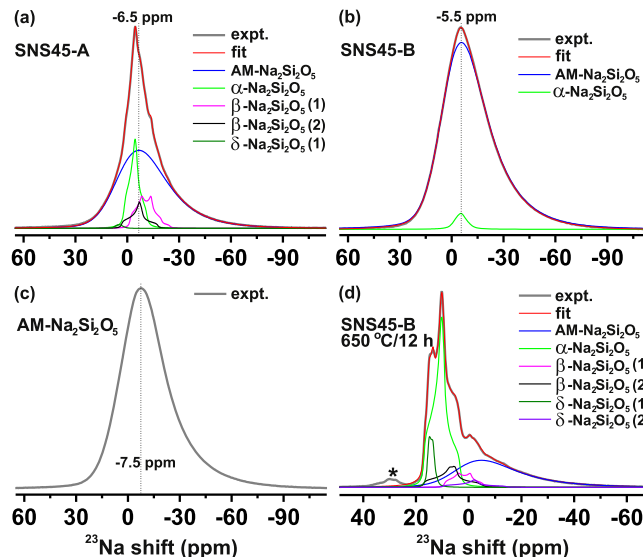


Fig. 2. ^{23}Na NMR spectra of SNS45-A, SNS45-B, AM- $\text{Na}_2\text{Si}_2\text{O}_5$, and SNS45-B 650 °C/12 h samples recorded with MAS frequency of 22 kHz. Spectral simulations are displayed together with the experimental spectra (Grey traces). Relevant phase assignments are marked by colour tags attached to each phase names. The best-fit parameters are listed in Table 2. Dotted vertical lines are used to indicate the peak positions of the AM- $\text{Na}_2\text{Si}_2\text{O}_5$ phase. Asterisk (*) sign marks the outer satellite transition. (For interpretation of the references to colour in this figure legend, the reader is referred to the web version of this article.)

deconvoluted the ^{23}Na spectra using DM-fit program [21]. To model the glass/amorphous phase, Czjzek [25] and Gaussian distributions (with LB denoting the FWHM in ppm) were assumed (CzSimple model in DMfit program) and average isotropic ^{23}Na chemical shift (δ_{iso}), and root-mean-square (rms) quadrupolar product $C_{Q\eta} = C_Q \sqrt{1 + \eta^2/3}$ have been estimated. Here C_Q and η denote the quadrupolar coupling constant and asymmetry parameter of the electric field gradient tensor, respectively. This model was implemented earlier extensively to analyse quadrupolar spectrum in disordered solids [26–29]. All other crystalline phases were modelled with second order quadrupolar line shape (Q MAS 1/2 in Dmfit program) to obtain the parameters δ_{iso} , C_Q , and η . During fitting, the parameters δ_{iso} , $C_{Q\eta}$, and LB associated with the amorphous phase and δ_{iso} , C_Q and η associated with the crystalline phases were allowed to evolve freely. The best-fit results are listed in Table 2.

The experimental ^{23}Na MAS NMR spectrum of pure AM- $\text{Na}_2\text{Si}_2\text{O}_5$ shown in Fig. 2(c) indicates an essentially amorphous line shape with no other components present. In the case of samples SNS45-A [Fig. 2(a)] and SNS45-B [Fig. 2(b)] the fitting procedure yields a broad signal with the mean isotropic shift $\delta_{\text{iso}} \approx 4.0, 4.1$ ppm, the quadrupolar product $C_{Q\eta} \approx 3.09, 3.03$ MHz, and LB $\approx 23.0, 20.0$ ppm for the samples of SNS45-A and SNS45-B, respectively. The fitting provided a lineshape for this amorphous part that compared well with that of the pure AM- $\text{Na}_2\text{Si}_2\text{O}_5$ sample shown in Fig. 2(c). Based on the above observations, we assigned the broad component in samples SNS45-A and SNS45-B as arising from the AM- $\text{Na}_2\text{Si}_2\text{O}_5$ phase. The FWHM, denoted by LB, of the amorphous component in SNS45-A is slightly higher compared to SNS45-B, indicating a higher degree of glass network disorder in the sample of SNS45-A. This result is consistent with the result obtained from ^{29}Si NMR where the FWHM of the peak corresponding to the Q³-units of AM- $\text{Na}_2\text{Si}_2\text{O}_5$ phase was noticed to be higher in SNS45-A compared to that of SNS45-B. Other than the broad AM- $\text{Na}_2\text{Si}_2\text{O}_5$ phase in ^{23}Na MAS NMR spectrum of SNS45-A, four peaks associated with crystalline phases are identified at $\delta_{\text{iso}} \approx \{1.8, -0.8, 3.3, 8.0\}$ ppm and with $C_Q \approx \{1.80, 2.52, 2.24, 1.46\}$ MHz, and $\eta \approx \{0.94, 0.52, 1.0, 0.55\}$. On the other hand, in SNS45-B only one minor crystalline phase contribution is obtained with $\delta_{\text{iso}} \approx -0.5$ ppm, $C_Q \approx 1.69$ MHz, and $\eta \approx 0.71$. We identify these crystalline phases as the early devitrification products.

The experimental ^{23}Na NMR spectrum of SNS45-B 650 °C/12 h displayed in Fig. 2(d) clearly shows that the major amorphous phase of the SNS45-B sample has been devitrified into several crystalline phases. The fit of the overall lineshape lead to the identification of the remaining part of the AM- $\text{Na}_2\text{Si}_2\text{O}_5$ phase, providing a broad peak

with $\delta_{\text{iso}} = 3.9$ ppm, $C_{Q\eta} = 2.95$ MHz and LB = 16.3 ppm, along with five extra peaks corresponding to different crystalline phases. Based on the previous reports [18,23,24,30], the peak with the set of parameters $\{\delta_{\text{iso}}, C_Q, \eta\} \approx \{17.0$ ppm, 1.85 MHz, 0.93} is assigned as crystalline $\alpha\text{-Na}_2\text{Si}_2\text{O}_5$ phase. The pair of peaks that appear at $\delta_{\text{iso}} \approx 9.9$ and 17.2 ppm with $C_Q \approx 2.27, 2.40$ MHz and $\eta \approx 0.50, 0.83$ respectively are from two non-equivalent Na sites in crystalline $\beta\text{-Na}_2\text{Si}_2\text{O}_5$ phase [designated as $\beta\text{-Na}_2\text{Si}_2\text{O}_5$ (1) and $\beta\text{-Na}_2\text{Si}_2\text{O}_5$ (2), respectively]. The other pair of peaks identified with $\delta_{\text{iso}} \approx 16.0$ and 9.8 ppm with $C_Q \approx 1.09, 2.40$ MHz and $\eta \approx 0.27, 0.98$ respectively are from two non-equivalent Na sites in crystalline $\delta\text{-Na}_2\text{Si}_2\text{O}_5$ phase [designated as $\delta\text{-Na}_2\text{Si}_2\text{O}_5$ (1) and $\delta\text{-Na}_2\text{Si}_2\text{O}_5$ (2) respectively]. Thus the present results are consistent with ^{29}Si MAS NMR results where also one could identify peaks corresponding to the $\alpha, \beta, \delta\text{-Na}_2\text{Si}_2\text{O}_5$ crystalline phases along with the broad line corresponding to the AM- $\text{Na}_2\text{Si}_2\text{O}_5$ phase. From comparison of quadrupolar parameters of SNS45-A and SNS45-B 650 °C/12 h, one may attribute the four additional peaks detected in SNS45-A correspond to $\alpha\text{-Na}_2\text{Si}_2\text{O}_5$, $\beta\text{-Na}_2\text{Si}_2\text{O}_5$, and $\delta\text{-Na}_2\text{Si}_2\text{O}_5$ phases but with different coordination environments resulting in different isotropic chemical shift positions. Similarly, the small signal in the ^{23}Na NMR spectrum of SNS45-B with parameters $\{\delta_{\text{iso}}, C_Q, \eta\} \approx \{-0.5$ ppm, 1.69 MHz, 0.71} may be identified as the contribution of $\alpha\text{-Na}_2\text{Si}_2\text{O}_5$ phase.

To confirm the phase identification hypothesis in the SNS materials, we conducted ^{23}Na two dimensional triple quantum MAS (3QMAS) NMR experiment which is a well-established method [31,32] to separate out overlapped resonances due to different Na species. Fig. 3 displays the 2D 3QMAS NMR spectra of SNS45-A and SNS45-B 650 °C/12 h samples. For each of the Na species, the slices parallel to the direct dimension (δ_2) were extracted and these are also shown in Fig. 3 on the right panel along with the corresponding fits with the relevant NMR parameters. The best-fit data are listed in Table 2. In SNS45-A [Fig. 3(a)] two separate signals are detected, one of which is the superposition of the signals due to the crystalline $\alpha\text{-Na}_2\text{Si}_2\text{O}_5$ and $\beta\text{-Na}_2\text{Si}_2\text{O}_5$ (2) phases. The second signal is identified as the crystalline $\beta\text{-Na}_2\text{Si}_2\text{O}_5$ (1) phase. Low signal-to-noise ratio limits the observation of separate peaks corresponding to $\delta\text{-Na}_2\text{Si}_2\text{O}_5$ phase in 3QMAS spectrum of SNS45-A. The C_Q and η values determined from the slices are consistent with the values obtained from 1D MAS spectrum. 3QMAS spectrum of SNS45-B 650 °C/12 h sample, displays clear signal contributions of crystalline $\alpha\text{-Na}_2\text{Si}_2\text{O}_5$, $\beta\text{-Na}_2\text{Si}_2\text{O}_5$ (1), $\beta\text{-Na}_2\text{Si}_2\text{O}_5$ (2), and $\delta\text{-Na}_2\text{Si}_2\text{O}_5$ (1) phases. Moreover, 3QMAS spectrum recorded on both the samples do not display any separate resonance which could be identified as AM- $\text{Na}_2\text{Si}_2\text{O}_5$ phase. This is possibly due to the fact that the amorphous phase (AM- $\text{Na}_2\text{Si}_2\text{O}_5$) has a broad line-shape which

Table 2
Results of ^{23}Na MAS NMR in the SNS45 samples.^a

Compound	Phases	One-pulse (1D)					3QMAS (2D)		
		Relative intensity $\pm 2.0\%$	$\delta_{\text{iso}} \pm 0.5$ ppm	$C_Q \pm 0.1$ MHz	η	$C_{Q\eta} \pm 0.2$ MHz	$\delta_{\text{iso}} \pm 0.8$ ppm	$C_Q \pm 0.1$ MHz	η
SNS45-A	AM- $\text{Na}_2\text{Si}_2\text{O}_5$	69.1	4.0	N/A	N/A	3.09	N/A	N/A	N/A
	$\alpha\text{-Na}_2\text{Si}_2\text{O}_5$	15.2	1.8	1.80	0.94	N/A	1.0	1.79	0.89
	$\beta\text{-Na}_2\text{Si}_2\text{O}_5$ (1)	9.2	-0.8	2.52	0.52	N/A	-4.5	2.29	0.48
	$\beta\text{-Na}_2\text{Si}_2\text{O}_5$ (2)	5.5	3.3	2.24	1.00	N/A	1.0	2.12	0.99
	$\delta\text{-Na}_2\text{Si}_2\text{O}_5$ (1)	1.0	8.0	1.46	0.55	N/A	N/A	N/A	N/A
SNS45-B	AM- $\text{Na}_2\text{Si}_2\text{O}_5$	97.8	4.1	N/A	N/A	3.03	N/A	N/A	N/A
	$\alpha\text{-Na}_2\text{Si}_2\text{O}_5$	2.2	-0.5	1.69	0.71	N/A	N/A	N/A	N/A
SNS45-B 650 °C/12 h	AM- $\text{Na}_2\text{Si}_2\text{O}_5$	33.9	3.9	N/A	N/A	2.95	N/A	N/A	N/A
	$\alpha\text{-Na}_2\text{Si}_2\text{O}_5$	42.4	17.0	1.85	0.93	N/A	16.7	1.80	0.9
	$\beta\text{-Na}_2\text{Si}_2\text{O}_5$ (1)	5.8	9.9	2.27	0.50	N/A	10.4	2.35	0.47
	$\beta\text{-Na}_2\text{Si}_2\text{O}_5$ (2)	8.8	17.2	2.40	0.83	N/A	16.6	2.44	0.8
	$\delta\text{-Na}_2\text{Si}_2\text{O}_5$ (1)	6.3	16.0	1.09	0.27	N/A	16.0	1.11	0.23
	$\delta\text{-Na}_2\text{Si}_2\text{O}_5$ (2)	2.8	9.8	2.40	0.98	N/A	N/A	N/A	N/A

^a The accuracy of the parameters relative intensity, δ_{iso} , C_Q , and $C_{Q\eta}$ are given as the bounds. For values outside this range a good fit was not possible.

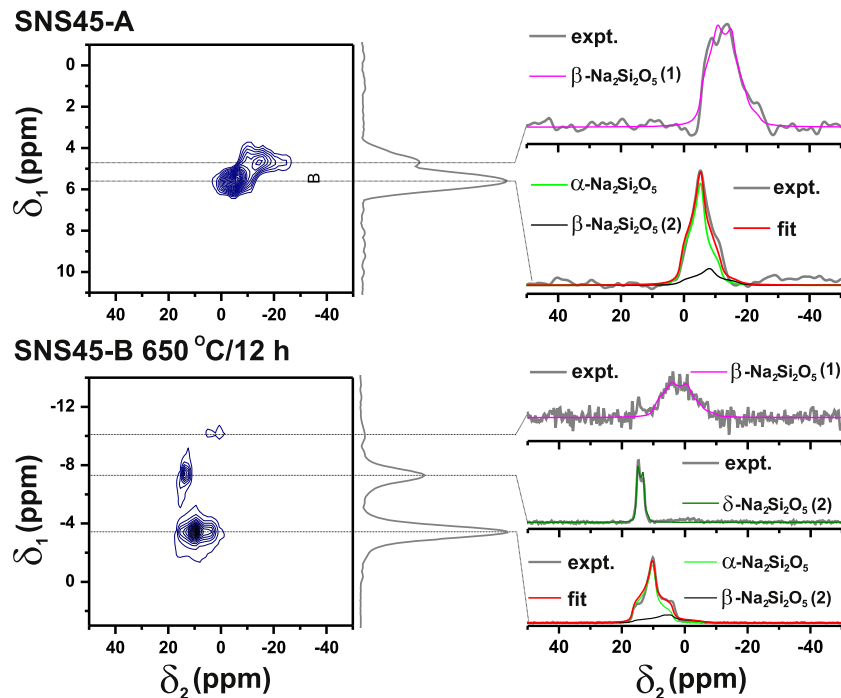


Fig. 3. ^{23}Na 3QMAS NMR spectra obtained at 11.7 T and 22 kHz MAS from SNS45-A (top) and SNS45-B 650 °C/12 h (bottom), shown together with cross sections (extracted parallel to δ_2) for each of the Na species; the corresponding fits with relevant phases are also shown at the right side of each 2D spectrum. (For interpretation of the references to colour in this figure legend, the reader is referred to the web version of this article.)

results in a short T_2 relaxation time. An analysis of the XRD patterns of the four samples are given in the Supplementary content and are in general agreement with the above observations based on NMR.

3.3. Phase composition-ionic conductivity correlation

The Arrhenius plots of conductivity in the temperature range of 300–500 °C is shown in Fig. 4 for the samples of SNS45-A, SNS45-B and SNS45-B 650 °C/12 h. Fig. 4 shows that the slope of the Arrhenius plot for all the three samples are similar. But the conductivity of SNS45-A is one order of magnitude higher compared to that of SNS45-B. The conductivity data of SNS45-B presented in Fig. 4 is in agreement with the data reported for the same nominal composition prepared by Tealdi et al. [10] whereas, the absolute value of conductivity of SNS45-A composition is in close agreement with the value obtained by Singh et al. [4]. The calculated conductivity values of SNS45-A and SNS45-B at 500 °C are 9.1×10^{-3} and $8.3 \times 10^{-4} \text{ S} \cdot \text{cm}^{-1}$, respectively. Present conductivity results thereby provide clear evidence that the absolute conductivity of SNS family may be significantly influenced by the synthesis conditions. Surprisingly, further enhancement of conductivity is observed in the devitrified SNS45-B 650 °C/12 h sample. The calculated conductivity value at 500 °C in this case is $1.9 \times 10^{-2} \text{ S} \cdot \text{cm}^{-1}$.

To understand the relationship between the phase compositions and ion conduction property in the SNS45 material, we recall the ^{29}Si and ^{23}Na results. ^{29}Si MAS NMR spectrum of SNS45-A and SNS45-B clearly revealed the presence of crystalline $\alpha\text{-SrSiO}_3$ phase and AM- $\text{Na}_2\text{Si}_2\text{O}_5$ phase. The highly conducting AM- $\text{Na}_2\text{Si}_2\text{O}_5$ phase part plays an important role in setting up a base Na^+ conductivity in SNS45-A and SNS45-B samples. In order to address the enhanced ionic conductivity obtained in the sample SNS45-A, we refer to ^{23}Na results which indicated the formation of glass-ceramic phase rather than a pure glass phase. In particular, SNS45-A is composed of a major glass/amorphous phase (AM- $\text{Na}_2\text{Si}_2\text{O}_5$) and minor devitrified phases (α -, β -, $\delta\text{-Na}_2\text{Si}_2\text{O}_5$). The relative content of these devitrified phases is higher in the SNS45-B 650 °C/12 h sample and correspondingly a further increase by an order of magnitude in conductivity is observed in this

material. Common glass-ceramics based on lithium silicate/sodium silicate/aluminosilicate crystalline phases have conductivities which are several orders of magnitude less than that of the base glass before crystallization. However, favourable structure for ionic transport can increase the conductivity of the composite by increasing the conductivity of the residual glass, even though the amount of that glass is only a small volume fraction of the composite. Such enhancement of Na^+ ion conductivity was recently observed in sulphide glass-ceramic [33,34] which was developed by recrystallization of glassy state. We observe a similar enhancement of Na^+ ion conductivity of the residual glass phase in SNS45-A and SNS45-B 650 °C/12 h samples.

4. Conclusions

The chemical phase composition-ionic conductivity relationship has been studied by multinuclear solid-state NMR and conductivity measurements. Our results confirm several expectations, but also offer some surprises. The NMR results clearly demonstrated that SNS45, bearing nominal composition of $\text{Sr}_{0.55}\text{Na}_{0.45}\text{SiO}_{2.775}$, consists of two phases. One being crystalline $\alpha\text{-SrSiO}_3$ with no Na doping, identified as

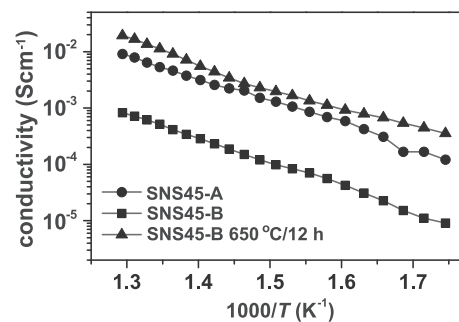


Fig. 4. Conductivity vs $1000/T$ plot for the samples of SNS45-A (solid circles) and SNS45-B (solid squares) with same nominal composition of $\text{Sr}_{0.55}\text{Na}_{0.45}\text{SiO}_{2.775}$ but prepared by different synthesis routes. Conductivity vs $1000/T$ plot for SNS45-B 650 °C/12 h sample is shown by solid triangles in the graph.

a narrow line only in the ^{29}Si spectra, and the other being a glass/amorphous $\text{Na}_2\text{O} \cdot 2\text{SiO}_2$ (AM- $\text{Na}_2\text{Si}_2\text{O}_5$) phase, as evidenced by the broad lines in both ^{29}Si and ^{23}Na NMR spectra. This finding is in agreement with the previous reports. The high ionic conductivity shown by the sample of SNS45 is therefore originated from the glass/amorphous $\text{Na}_2\text{O} \cdot 2\text{SiO}_2$ phase. The ^{23}Na NMR results of SNS45-A and SNS45-B indicated that different synthesis conditions strongly influence the degree of crystallization–amorphization of the system. High temperature treatment at 650 °C for longer duration of 12 h, followed by slow cooling to room temperature, devitrifies the amorphous $\text{Na}_2\text{O} \cdot 2\text{SiO}_2$ phase in $\text{Sr}_{0.55}\text{Na}_{0.45}\text{SiO}_{2.775}$ into different polymorphs of $\text{Na}_2\text{Si}_2\text{O}_5$. Both ^{29}Si and ^{23}Na NMR spectra clearly affirmed the presence of α -, β -, δ - $\text{Na}_2\text{Si}_2\text{O}_5$ in the devitrified form, SNS45-B 650 °C/12 h. The ^{23}Na NMR results also indicated the presence of α -, β -, δ - $\text{Na}_2\text{Si}_2\text{O}_5$ early crystalline phases in SNS45-A, but only α - $\text{Na}_2\text{Si}_2\text{O}_5$ phase in SNS45-B. Among α -, β -, and δ - $\text{Na}_2\text{Si}_2\text{O}_5$ phases, the δ - $\text{Na}_2\text{Si}_2\text{O}_5$ possess superior ion exchange properties relative to other phases [35]. Thus, in the sample of SNS45-A, the presence of early crystalline δ - $\text{Na}_2\text{Si}_2\text{O}_5$ phase along with early crystalline α -, β - $\text{Na}_2\text{Si}_2\text{O}_5$ phases grown within the glass/amorphous $\text{Na}_2\text{O} \cdot 2\text{SiO}_2$ phase domains possibly increases the ionic mobility along the grain boundaries in the glass-ceramic phase and thus enhances ionic conductivity. On the other hand, the enhancement of ionic conductivity observed in SNS45-B 650 °C/12 h may be attributed to a significant increase of the δ - $\text{Na}_2\text{Si}_2\text{O}_5$ phase. Further careful studies need to be done in the recrystallized Na-SrSiO₃ ionic conductors. Lastly, present study demonstrates the unique capability of solid-state NMR for identifying different crystalline and/or amorphous phases in the ion conducting materials leading to an understanding of the structure–property relationship in these materials.

Acknowledgement

The authors gratefully acknowledge the XRD facility of Physics Department and the NMR Research Centre, Indian Institute of Science, Bangalore for the spectrometer facility. They acknowledge Prof. K. B. R. Varma for extending facilities for the conductivity measurements and useful discussions and Mr. Gangaesh G. Velip and Miss Ankita Y. Shikerkar for their help in sample preparations. KVR acknowledges the Council of Scientific and Industrial Research, India, for the award of the Emeritus Scientist grant No. 21 (1018)/15/EMR-II. BP thanks the University Grants Commission for providing a startup grant F.4-5(117-FRP)/2014(BSR).

Appendix A. Supplementary data

Supplementary data related to this article can be found at <http://dx.doi.org/10.1016/j.ssnmr.2017.05.001>.

References

- [1] A.J. Jacobson, Materials for solid oxide fuel cells, *Chem. Mater.* 22 (2010) 660–674.
- [2] L. Malavasi, C.A.J. Fisher, M.S. Islam, Oxide-ion and proton conducting electrolyte materials for clean energy application: structural and mechanistic features, *Chem. Soc. Rev.* 39 (2010) 4370–4387.
- [3] A. Aguadero, L. Fawcett, S. Taub, R. Woolley, K.-T. Wu, N. Xu, J.A. Kilner, S. J. Skinner, Materials development for intermediate-temperature solid oxide electrochemical devices, *J. Mater. Sci.* 47 (2012) 3925–3948.
- [4] P. Singh, J.B. Goodenough, Monoclinic $\text{Sr}_{1-x}\text{Na}_x\text{SiO}_{3-0.5x}$: new superior oxide ion electrolytes, *J. Am. Chem. Soc.* 135 (2013) 10149–10154.
- [5] R. Martinez-Coronado, P. Singh, J. Alonso-Alonso, J.B. Goodenough, Structural investigation of the oxide-ion electrolyte with SrMo_3 ($M=\text{Si}/\text{Ge}$) structure, *J. Mater. Chem. A* 2 (2014) 4355–4360.
- [6] T. Wei, P. Singh, Y. Gong, J.B. Goodenough, Y. Huang, K. Huang, $\text{Sr}_{3-3x}\text{Na}_{3x}\text{Si}_3\text{O}_9 \cdot 1.5x$ ($x=0.45$) as a superior solid oxide-ion electrolyte for intermediate temperature-solid oxide fuel cells, *Energy Environ. Sci.* 7 (2014) 1680–1684.
- [7] R.D. Bayliss, S.N. Cook, S. Fearn, J.A. Kilner, C. Greaves, S.J. Skinner, On the oxide ion conductivity of potassium doped strontium silicates, *Energy Environ. Sci.* 7 (2014) 2999–3005.
- [8] R.D. Bayliss, S.N. Cook, D.O. Scanlon, S. Fearn, J. Cabana, C. Greaves, J.A. Kilner, S.J. Skinner, Understanding the defect chemistry of alkali metal strontium silicate solid solutions: insights from experiment and theory, *J. Mater. Chem. A* 2 (2014) 17919–17924.
- [9] I.R. Evans, J.S.O. Evans, H.G. Davies, A.R. Haworth, M.L. Tate, On $\text{Sr}_{1-x}\text{Na}_x\text{SiO}_{3-0.5x}$: new superior fast ion conductors, *Chem. Mater.* 26 (2014) 5187–5189.
- [10] C. Tealdi, L. Malavasi, I. Uda, C. Ferrara, V. Berbenni, P. Mustarelli, Nature of conductivity in SrSiO_3 -based fast ion conductors, *Chem. Commun.* 50 (2014) 14732–14735.
- [11] Y. Jee, X. Zhao, K. Huang, On the cause of conductivity degradation in sodium strontium silicate ionic conductor, *Chem. Commun.* 51 (2015) 9640–9642.
- [12] X. Lei, Y. Jee, K. Huang, Amorphous $\text{Na}_2\text{Si}_2\text{O}_5$ as a fast Na^+ conductor: an ab initio molecular dynamics simulation, *J. Mater. Chem. A* 3 (2015) 19920–19927.
- [13] J.R. Peet, C.M. Widdifield, D.C. Apperley, P. Hodgkinson, M.R. Johnson, I. R. Evans, Na^+ mobility in sodium strontium silicate fast ion conductors, *Chem. Commun.* 51 (2015) 17163–17165.
- [14] P.-H. Chien, Y. Jee, C. Huang, R. Dervisoglu, I. Hung, Z. Gan, K. Huang, Y.-Y. Hu, On the origin of high ionic conductivity in Na-Doped SrSiO_3 , *Chem. Sci.* 7 (2016) 3667–3675.
- [15] K. Sood, S. Basu, Co-existence of amorphous and crystalline phases in Na-Doped SrSiO_3 system, *RSC Adv.* 6 (2016) 20211–20218.
- [16] Y. Jee, X. Zhao, X. Lei, K. Huang, Phase relationship and ionic conductivity in Na-SrSiO₃ ionic conductor, *J. Am. Ceram. Soc.* 99 (2016) 324–331.
- [17] K.K. Inglis, J.P. Corley, P. Florian, J. Cabana, R.D. Bayliss, F. Blanc, Structure and sodium ion dynamics in sodium strontium silicate investigated by multi-nuclear solid state NMR, *Chem. Mater.* 28 (2016) 3850–3861.
- [18] K.J.D. Mackenzie, M.E. Smith, Multinuclear solid-state NMR of inorganic materials, *Pergamon Mater. Ser.* 6 (2002).
- [19] S.E. Ashbrook, S. Sneddon, New methods and applications in solid-state NMR spectroscopy of quadrupolar nuclei, *J. Am. Chem. Soc.* 136 (2014) 15440–15456.
- [20] M. Eden, NMR studies of oxide-based glasses, *Annu. Rep. Prog. Chem. Sect. C. Phys. Chem.* 108 (2012) 177–221.
- [21] D. Massiot, F. Fayon, M. Capron, I. King, S.L. Calve, B. Alonso, J.O. Durand, B. Bujoli, Z. Gan, G. Hoatson, Modelling one and two dimensional solid-state NMR spectra, *Magn. Reson. Chem.* 40 (2002) 70–76.
- [22] J.B. Murdoch, J.F. Stebbins, I.S.E. Carmichael, High-resolution ^{29}Si NMR study of silicate and aluminosilicate glasses: the effect of network-modifying cations, *Am. Mineral.* 70 (1985) 332–343.
- [23] D. Heidemann, C. Hübert, W. Schwieger, P. Grabner, K.-H. Bergk, P. Sarv, ^{29}Si -Und ^{23}Na -Festkörper-MAS-NMR-Untersuchungen an Modifikationen des $\text{Na}_2\text{Si}_2\text{O}_5$, *Z. Anorg. Allg. Chem.* 617 (1992) 169–177.
- [24] X. Xue, J.F. Stebbins, ^{23}Na NMR chemical shifts and local Na coordination environments in silicate crystals, melts and glasses, *Phys. Chem. Min.* 20 (1993) 297–307.
- [25] G. Czjzek, J. Fink, F. Götz, H. Schmidt, J.M.D. Coey, J.P. Rebouillat, A. Liénard, Atomic coordination and the distribution of electric-field gradients in amorphous solids, *Phys. Rev. B* 23 (1981) 2513–2530.
- [26] D.R. Neuville, L. Cormier, D. Massiot, Al environment in tectosilicate and peraluminous glasses: a ^{27}Al MQ-MAS NMR, Raman, and XANES investigation, *Geochim. Cosmochim. Acta* 68 (2004) 5071–5079.
- [27] P. Florian, N. Sadiki, D. Massiot, J.P. Coutures, ^{27}Al NMR study of the structure of lanthanum- and yttrium-based aluminosilicate glasses and melts, *J. Phys. Chem. B* 111 (2007) 9747–9757.
- [28] B. Pahari, S. Iftekhar, A. Jaworski, K. Okhotnikov, K. Jansson, B. Stevensson, J. Grins, M. Edén, Composition–property–structure correlations of scandium aluminosilicate glasses revealed by multinuclear ^{45}Sc , ^{27}Al , and ^{29}Si solid-state NMR, *J. Am. Ceram. Soc.* 95 (2012) 2545–2553.
- [29] S. Iftekhar, B. Pahari, K. Okhotnikov, A. Jaworski, B. Stevensson, J. Grins, M. Edén, Properties and structures of $\text{RE}_2\text{O}_3 \cdot \text{Al}_2\text{O}_3 \cdot \text{SiO}_2$ ($\text{RE}=\text{Y}, \text{Lu}$) glasses probed by molecular dynamics simulations and solid-state NMR: the roles of aluminium and rare-earth ions for dictating the microhardness, *J. Phys. Chem. C* 116 (2012) 18394–18406.
- [30] H. Koller, G. Engelhardt, A.P.M. Kentgens, J. Sauer, ^{23}Na NMR spectroscopy of solids: interpretation of quadrupole interaction parameters and chemical shifts, *J. Phys. Chem.* 98 (1994) 1544–1551.
- [31] L. Frydman, J.S. Harwood, Isotropic spectra of half-integer quadrupolar spins from Bidimensional magic-angle-spinning NMR, *J. Am. Chem. Soc.* 117 (1995) 5367–5368.
- [32] J.P. Amoureaux, C. Fernandez, S. Steuernagel, Z filtering in MQMAS NMR, *J. Magn. Reson. A* 123 (1996) 116–118.
- [33] A. Hayashi, K. Noi, A. Sakuda, M. Tatsumisago, Superionic glass-ceramic electrolytes for room-temperaturre rechargeable sodium Batteries, *Nat. Commun.* 3 (2012) 856–860.
- [34] A. Hayashi, K. Noi, N. Tanibata, M. Nagao, M. Tatsumisago, High sodium ion conductivity of glass-ceramic electrolytes with cubic Na_3PS_4 , *J. Power Sources* 258 (2014) 420–423.
- [35] V. Kahlenberg, G. Dörsam, M. Wendschuh-Josties, R.X. Fischer, The crystal structure of δ - $\text{Na}_2\text{Si}_2\text{O}_5$, *J. Solid State Chem.* 146 (1999) 380–386.